Electronic Supplementary Material (ESI) for Physical Chemistry Chemical Physics.
This journal is © the Owner Societies 2016

# Supplementary Information: Why do Proton Conducting Polybenzimidazole Phosphoric Acid Membranes perform well in High-temperature PEM Fuel Cells?

Jan-Patrick Melchior, Günter Majer and Klaus-Dieter Kreuer

## 1 Experimental

**Thermogravimetric Analysis (TGA) - Humidification** A humidified TGA set up[9] was used to determine the equilibrium water uptake of phosphoric acid and phosphoric acid benzimidazole mixtures. In all cases nominally dry $H_3PO_4$ was used as a reference for $\lambda = 3$. A constant $N_2$ gas flow is led through water in a temperature controlled vessel (see figure 1) to ensure saturation of the gas. The water saturated gas is then led to the *sample chamber*, where the sample is placed in a teflon crucible magnetically coupled to a balance. Spatial separation of humidifier and sample chamber by the temperature controlled *transfer zone* ensures independent temperature control in the two compartments. With the temperature (in Celsius) in both humidifier $T_W$ and sample chamber $T_S$ the saturation partial water pressure in the respective compartments $e_W$ and $e_S$ are calculated according to the empirical equations:

$$\begin{aligned} e_{W,S}(T_{W,S}(^\circ C)) &= 6.1078 \cdot 10^{7.5 \cdot T_i/(237.3+T_i)} \text{ hPa} ; & T < 70^\circ C \\ e_{W,S}(T_{W,S}(^\circ C)) &= 5.94062 \cdot 10^{7.28829 \cdot T_i/(226.531+T_i)} \text{ hPa} ; & T > 70^\circ C \end{aligned} \quad (1)$$

obtained from a fit to literature data.[10] The relative humidity ($RH$) is calculated from the ratio of saturation water pressure in both chambers:

$$RH = \frac{e_W}{e_S} \cdot 100\% \quad (2)$$

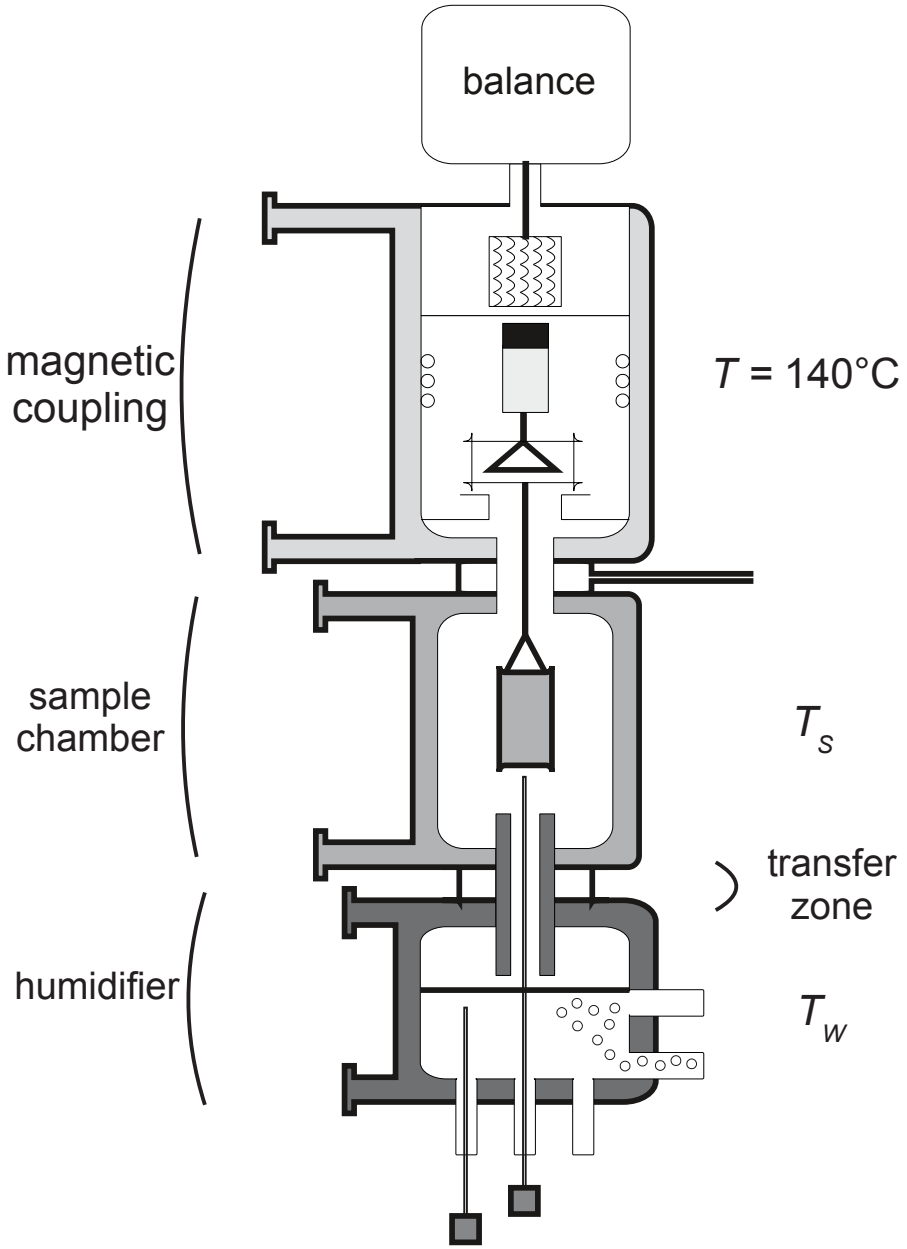


Figure 1: Schematic of inhouse build TGA device (see also [9]) with balance magnetically coupled to a crucible containing the sample in the temperature controlled sample chamber which is humidified through a constant gas stream $N_2$ bubbling through the temperature controlled humidifier containing water. The compartments are separated by the transferzone to ensure independent temperature control in the compartments. All flanges connecting the different parts are temperature controlled as to prevent condensation of water.

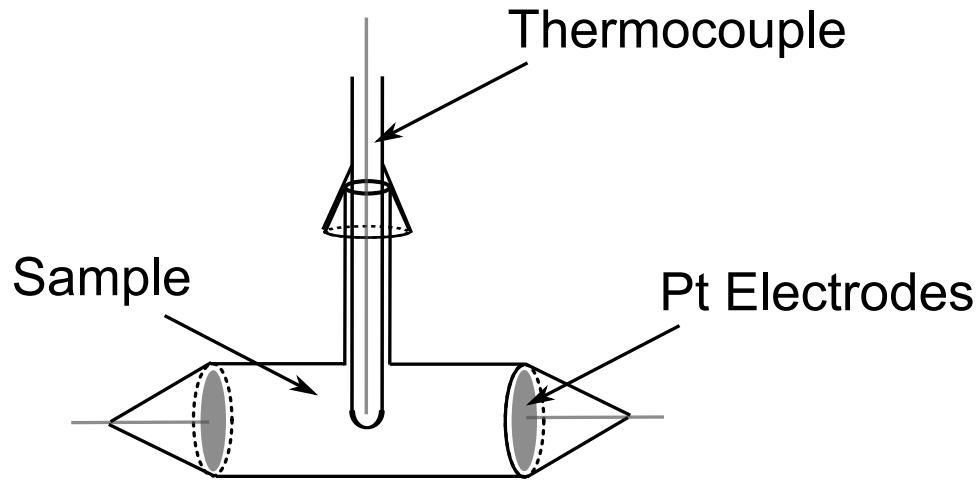


Figure 2: Schematic of the T-shaped impedance cell including a type K thermocouple and Pt electrodes to either side.

**Impedance Cell** Impedance spectroscopy experiments are conducted in a pseudo-four-point setting in a T-shaped Duran glass cell (figure 2) with two circular platinum electrodes. The sample chamber ($V \sim 3$ml) is filled through a central tapping socket which is sealed gas tight during the temperature dependent measurement by a glas insert containing a typ K thermocouple trough which temperature is controlled. Temperatures above $T = 60°C$ have been set in a Memmert ULE 400 oven and temperatures below $T = 60°C$ in a Lauda RE207 thermostat.

**Equilibrium at low water contents** The multitude of condensation and dissociation equilibria in phosphoric acid make extended equilibration times necessary. For neat phosphoric acid complete compositional equilibrium is reached after weeks at its melting point.[12] This estimate has been confirmed by measuring the $^{17}O$ exchange between $H_2O$ and $H_3PO_4$ which takes place through condensation reactions. For lower water contents even longer equilibration times can be expected and equilibrium compositions of higher temperatures are "frozen in" by fast cooling of the sample. As already pointed out by Munson in 1964 this might be the reason for the severe difference between compositional data for neat $H_3PO_4$ obtain by Munson [12] ($\sim 2\%H_2O$) and by Huhiti et. al.[3] and Jameson[4] ($\sim 6\%H_2O$). In this work compositions have therefore only be analyzed by $^{31}$P-NMR at elevated temperatures ($T > 70°$C). Extrapolation towards lower temperatures reproduces the data of Munson. On the other hand, stable conductivity, diffusion and $T_1$ relaxation times are reached at much lower equilibration times and despite non-equilibrium compositions.

**Calculations including phosphoric acid's density** In calculating $\sigma^D_{vehicle}$ and $\sigma^D_{structure}$ temperature dependent density values for different water contents are used. Summaries of physical properties of $H_3PO_4$ (aq) can be found in the book of Slack [14], the DOE report of Sarangapani et al. [13], or more recently the article by Korte [8]. Of special importance for this study are the empirical equations for density as a function of temperature and water content. MacDonald and Boyack report an empirical equation; (W = weight percentage of $H_3PO_4$ (aq); T = Temperature in $°C$; valid in the range 86-102wt% $H_3PO_4$ (aq); 25-170 °C ):

$$\rho = 0.68235 + 1.20811 \cdot 10^{-2} W - \left(1.2379 \cdot 10^{-3} - 3.7938 \cdot 10^{-6} W\right) T \ \frac{g}{cm^3} \tag{3}$$

The data of Egan and Luff [2] and Christensen and Reed [1] (15-100wt% $H_3PO_4$ (aq); 25-60 °C) have been joined and fitted with the following equation:

$$\begin{aligned} \rho =& 0.959185 + 5.42201 \cdot 10^{-3} W + 2.264 \cdot 10^{-5} W^2 + 1.2172 \cdot 10^{-7} W^3 \\ & - (2.33111 \cdot 10^{-4} + 4.75028 \cdot 10^{-6} W) T + 2.43866 \cdot 10^{-6} T^2 \ \frac{g}{cm^3} \end{aligned} \tag{4}$$

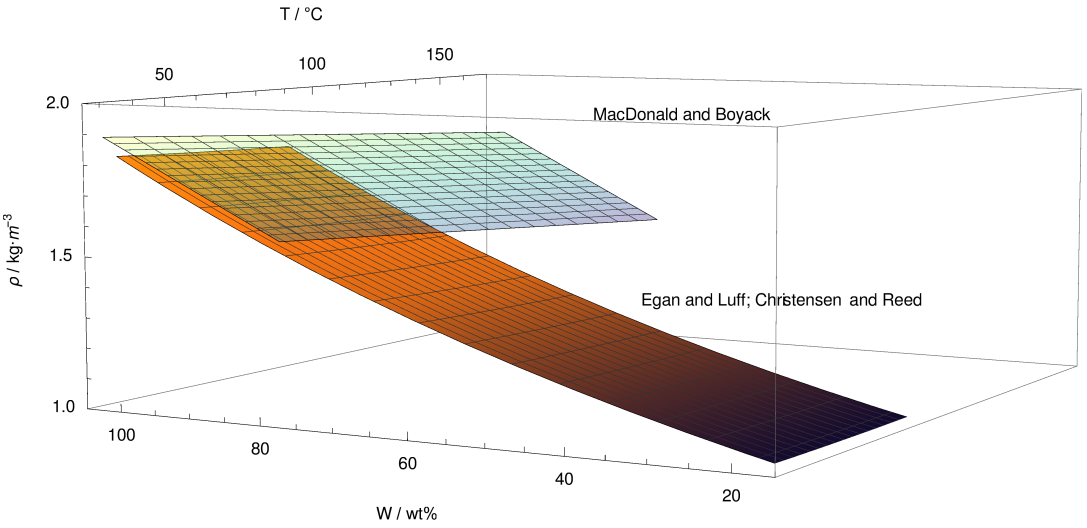


Figure 3: Visualization of empirical density equations by MacDonald and Boyack[11] (blue) and according to data of Egan and Luff [2]; Christensen and Reed [1].

Densities for the mixtures with benzimidazole and imidazole have been calculated through weighted summation of the temperature dependent $H_3PO_4$ density and (benz)imidazole densities ($\rho_{BI} = 1.23g \cdot cm^{-3}$; $\rho_{Imi} = 1.03g \cdot cm^{-3}$).[10]

# 2 Results

## 2.1 Composition

As pointed out in the main text frustration of the hydrogen bond network in nominally dry phosphoric acid and the investigated mixtures relaxes through condensation and protonation of the inherent water, or the protonation of the added Bronsted bases imidazole or benzimidazole. Therefore addition of imidazole and benzimidazole actually decreases the degree of condensation of phosphoric acid, i.e., the molar fraction of phosphoric acid condensates di-phosphoric acid, tri-phosphoric acid, etc. ($X_{P2}$, $X_{P2}$, etc.) and water $X_{aq}$ is reduced upon addition of (benz)imidazole and the molar fraction of ortho-phosphoric acid $X_{P1}$ is increased. We like to stress here that the molar fraction of ortho-phosphoric acid $X_{P1}$ is virtually identical in mixtures with the respective same amounts of benzimdiazole or imidazole (see figure 16), i.e., the amount of additional proton acceptors determines the molar fraction of ortho-phosphoric acid $X_{P1}$. This also holds true for addition of bisbenzimidazole[1] (see figure 4) which contains twice as many additional acceptor sites per molecule as (benz)imidazole and therefore mixtures with 6 mole phosphoric acid per bisbenzimidazole haven the same effective molar fraction of ortho-phosphoric acid $X_{P1}$ than mixtures with 3 mole phosphoric acid per (benz)imidazole (see figure 16).

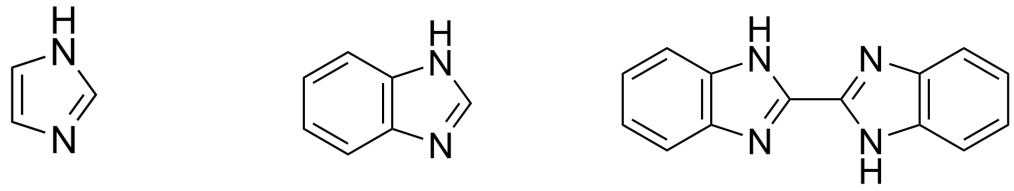

(a) Imidazole (Imi) (b) Benzimidazole (BI) (c) Bisbenzimidazole (BisBI)

Figure 4: Basic additives used in mixtures with phosphoric acid and their respective abbreviations.

[1] We thank Alexander Gulledge (University of South Carolina) for providing the bisbenzimidazole.

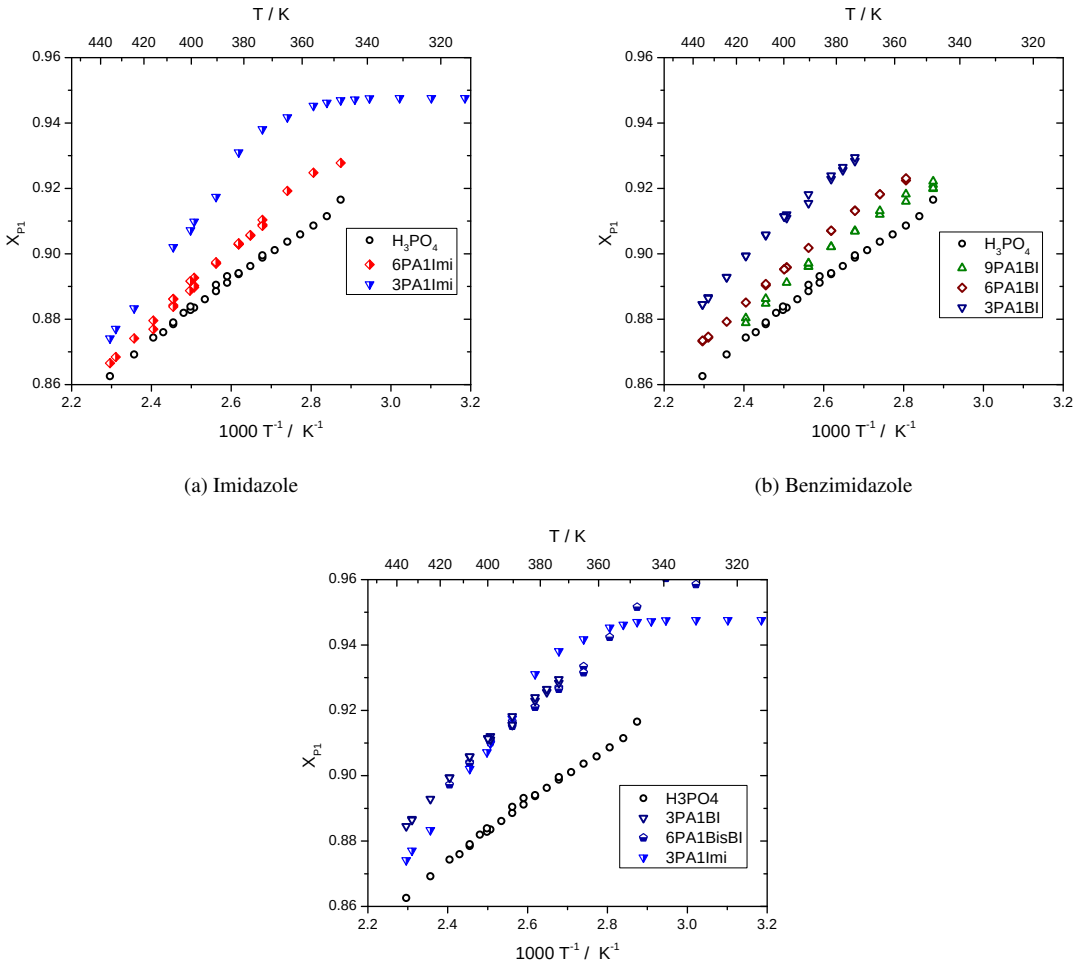


(a) Imidazole

(b) Benzimidazole

(c) Different additives with $\chi = 0.333$

Figure 5: Molar fraction of ortho-phosphoric acid $X_{P1}$ in the PA-part of nominally dry phosphoric acid mixed with a) imidazole and b) benzimidazole at different additive content and c) for different additives with the same ratio of imidazole units to phosphoric acid $\chi$. Addition of basic groups increases $X_{P1}$ in the PA-part and decreases the water content.

## 2.2 Conductivity

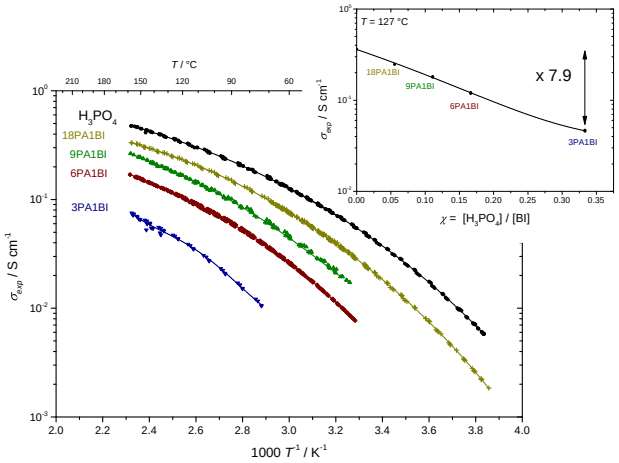


Figure 6: Conductivity measured for different benzimidazole content for nominally dry $H_3PO_4$.

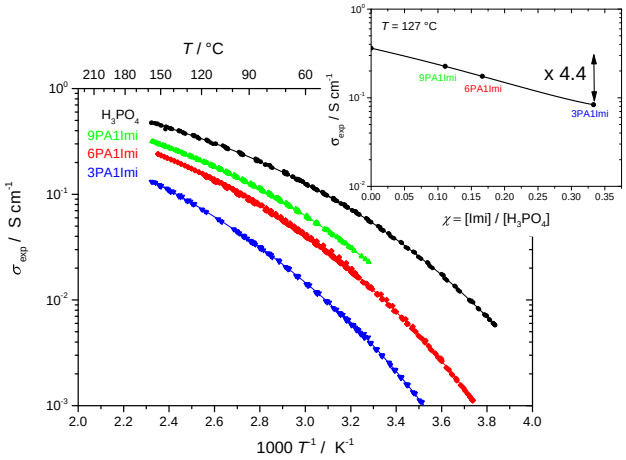


Figure 7: Conductivity measured for different benzimidazole content for nominally dry $H_3PO_4$.

## 2.3 Diffusion

The diffusion coefficients for the different samples nominally dry $H_3PO_4$ ($H_3PO_4$), 9 Phosphoric Acid · Benzimidazole (9PA1BI), 6 Phosphoric Acid · Benzimidazole (6PA1BI), 3 Phosphoric Acid · Benzimidazole (3PA1BI), 6 Phosphoric Acid · Imidazole (6PA1Imi), and 3 Phosphoric Acid · Imidazole (3PA1Imi) are shown in the following figures. Proton diffusion coefficients in the mixtures have been obtained through the Kärger equations as described in the main part of the text.

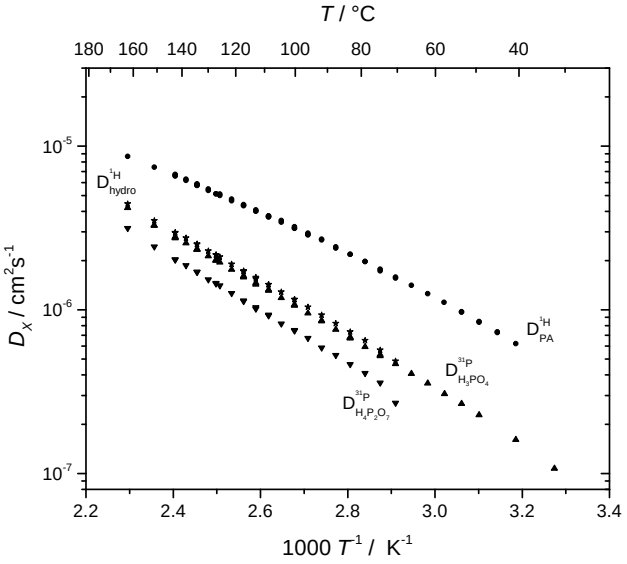


Figure 8: Diffusion coefficients for the different phosphoric acid species and protons for $H_3PO_4$.

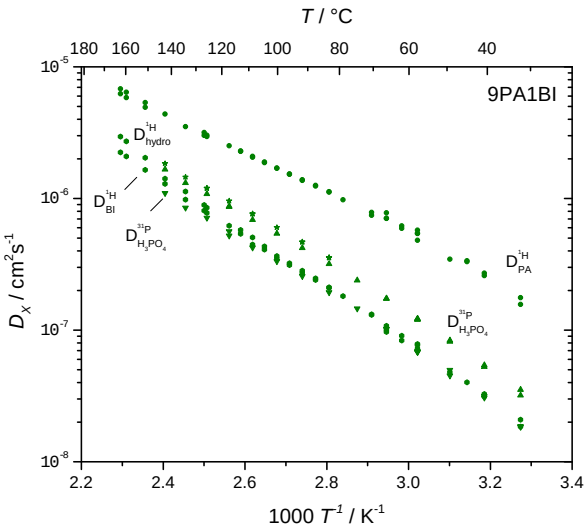


Figure 9: Diffusion coefficients for the different phosphoric acid species, benzimidazole, and protons for 9PA1BI.

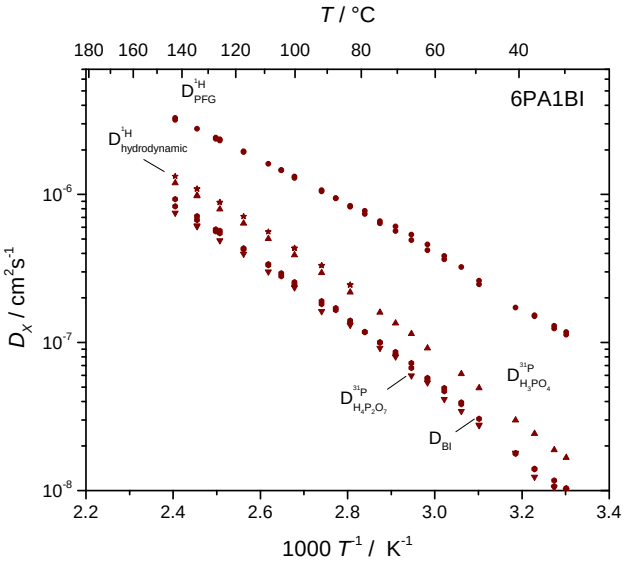


Figure 10: Diffusion coefficients for the different phosphoric acid species, benzimidazole, and protons for 6PA1BI.

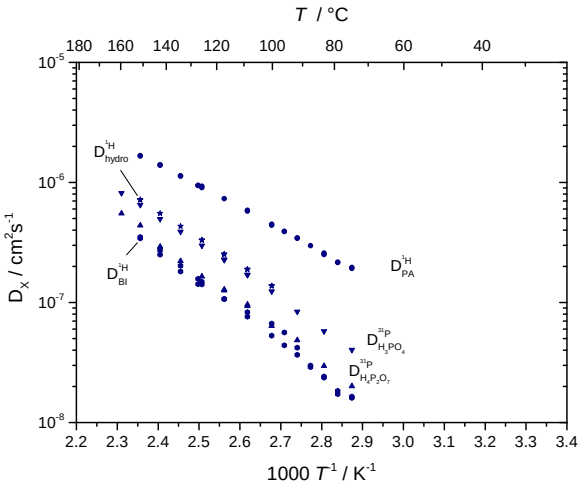


Figure 11: Diffusion coefficients for the different phosphoric acid species, benzimidazole, and protons for 3PA1BI.

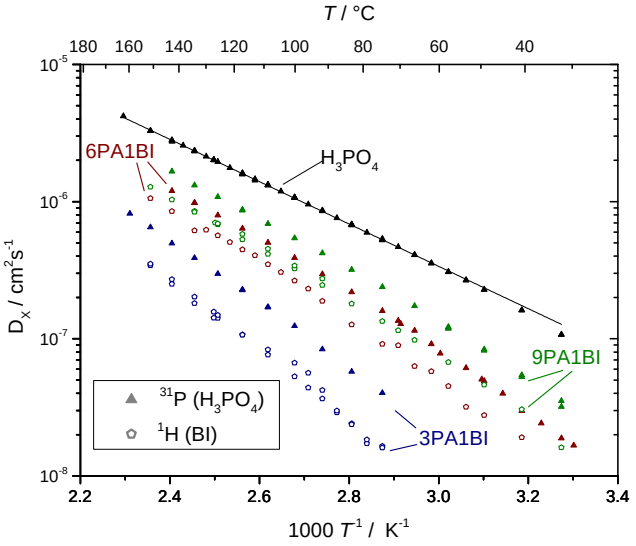


Figure 12: Diffusion coefficients for benzimidazole and orthophosphoric acid for 3PA1BI, 6PA1BI, and 9PA1BI.

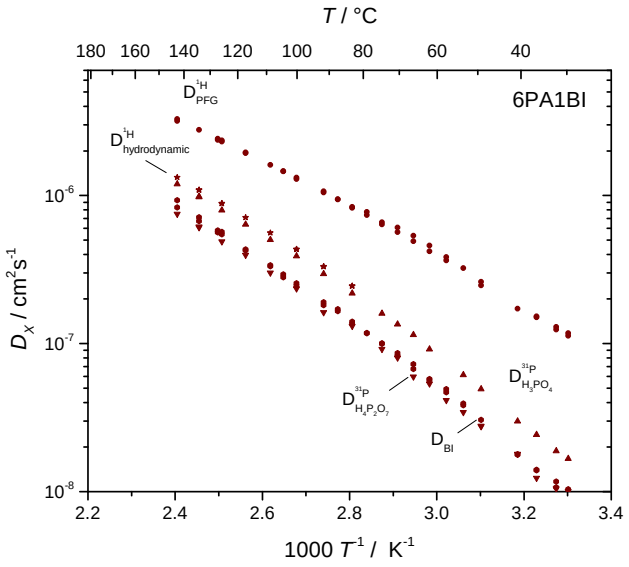


Figure 13: Diffusion coefficients for the different phosphoric acid species, and protons for 6PA1Imi.

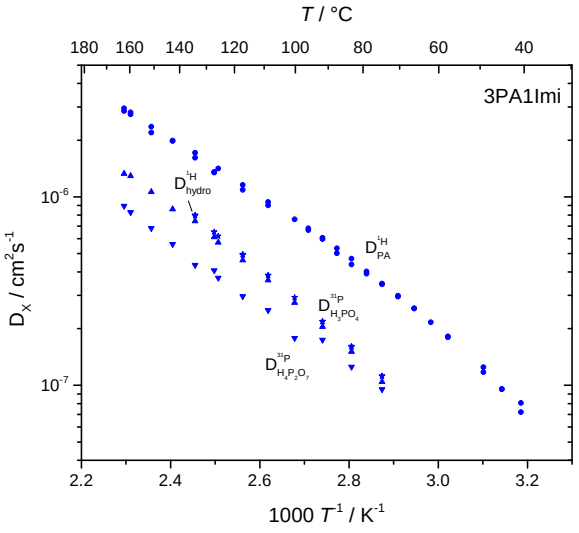


Figure 14: Diffusion coefficients for the different phosphoric acid species, and protons for 3PA1Imi.

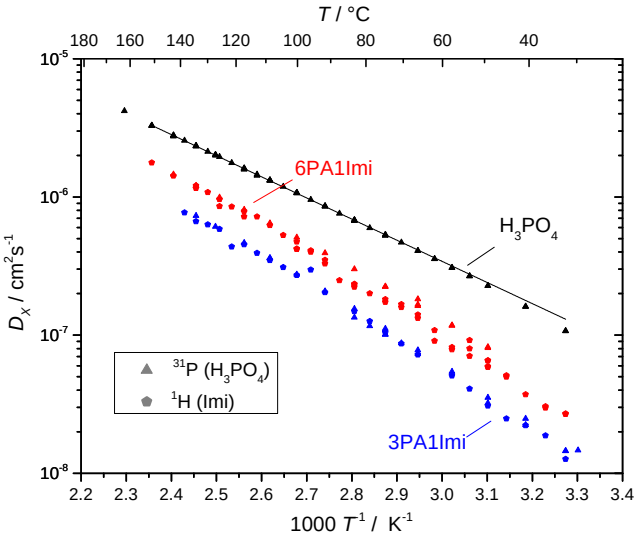


Figure 15: Diffusion coefficients for imidazole and orthophsophoric acid for 3PA1Imi and 6PA1Imi.

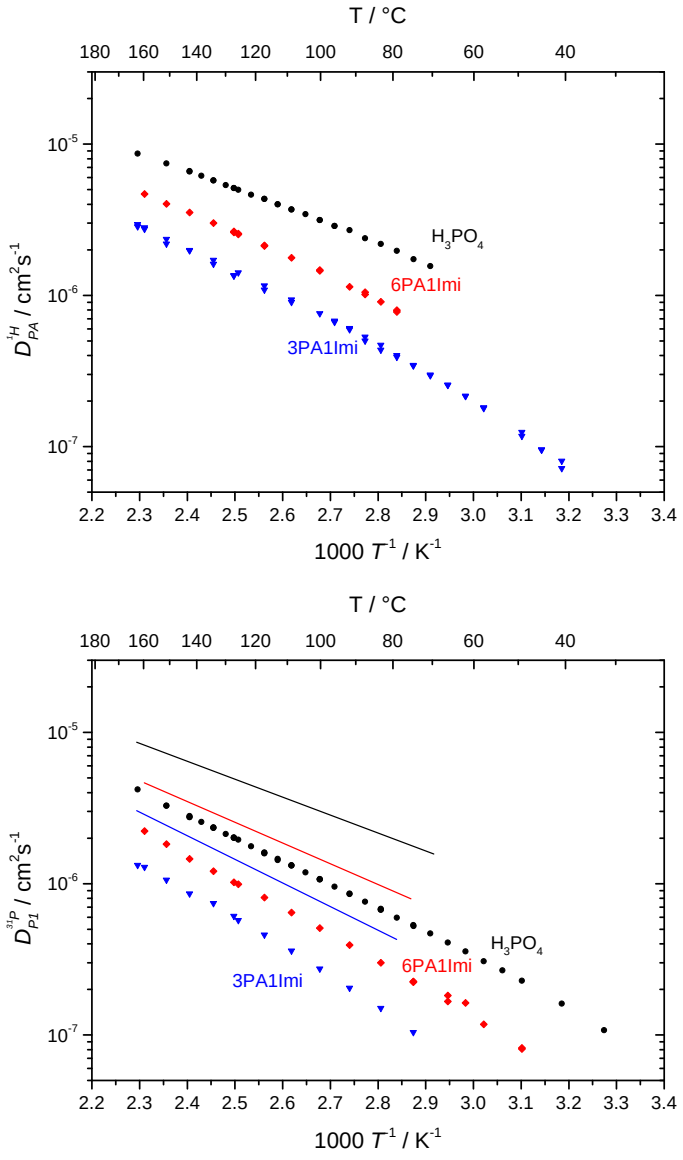


Figure 16: a) Diffusion coefficients for protons in the PA part of PA/Imi mixture $D_{PA}^{1H}$ as obtained from $^1$H-PFG NMR and b) diffusion coefficient of orthophosphate species $D_{P1}^{31P}$ for the same mixtures.

# 3 A Perspective on Exchange Effects in PFG-NMR Diffusion Measurements of PBI-PA membranes

By analysis of coalescing $^1$H NMR spectra, the lifetimes for proton exchange between $H_3PO_4$ and (benz)imidazole have been found to be on the same *millisecond* scale as the diffusion times $\Delta$ in $^1$H PFG-NMR. Accordingly the intermediate exchange model by Kärger [6, 7] was used to evaluate the decay of the echo intensity (see main text). Such exchange rates have not been reported for PBI-PA membranes before and in previous studies by PFG-NMR [5, 15] the Stejskal-Tanner equation was used to analyze the decay of the echo intensity. The relevant differences between evaluation of PFG-NMR echo attenuation with the Stejskal-Tanner or the Kärger model are briefly discussed.

## 3.1 Influence of Exchange on the Apparent Diffusion Coefficient in PA-BI Mixtures

On the intermediate exchange timescale the decay of the echo intensity $f$ depends on the diffusion coefficients of both exchange sites $D_a$ and $D_b$, their populations $p_a$ and $p_b$, and the exchange life times $\tau_a$ and $\tau_b$:

$$
\begin{aligned}
f &= p'_a e^{-b_i D'_a} + p'_b e^{-b_i D'_b} \qquad (5)\\
D'_{a,b} &= C_{1D} \mp C_{2D}\\
C_{1D} &= \frac{1}{2}\cdot\left(D_a + D_b + \frac{1}{\gamma^2\delta^2 G^2}\left(\frac{1}{\tau_a}+\frac{1}{\tau_b}\right)\right)\\
C_{2D} &= \frac{1}{2}\cdot\sqrt{\left(D_b - D_a + \frac{1}{\gamma^2\delta^2 G^2}\left(\frac{1}{\tau_b}-\frac{1}{\tau_a}\right)\right)^2 + \frac{1}{\gamma^4\delta^4 G^4}\frac{4}{\tau_a\tau_b}}\\
p'_b &= \frac{1}{D'_b - D'_a}\left(p_1 D_a + p_b D_b - D'_a\right)\ ;\ p'_a = 1 - p'_b
\end{aligned}
$$

The deviations of $D_a$ from the apparent diffusion coefficients $D_{app}$ obtained through the Stejskal-Tanner equation are estimated for the monomeric systems investigated in this work and for PBI-PA membranes in a short numerical simulation. Echo decay data were generated according to equation 5 by MATHEMATICA 10.0 and the Stejskal-Tanner equation was fitted by the least square fitting routines provided by the same program.

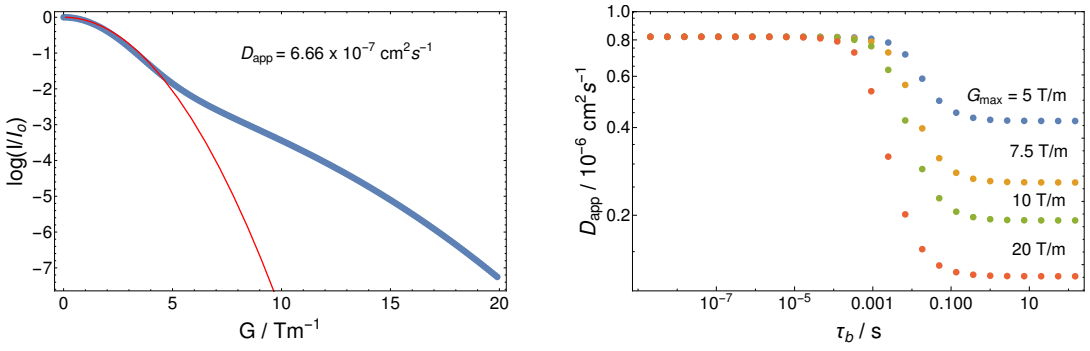


(a) Example fit

(b) $\tau_b$-dependence of $D_{app}$

Figure 17: a) The blue line shows data generated according to equation 5 for the model system described in the text with $\tau_b = 0.01\ s$, $\Delta = 0.04\ s$. The red line shows a fit of the Stejskal-Tanner equation to the generated data and corresponds to an apparent diffusion coefficient $D_{app} = 6.66 \cdot 10^{-7}\ cm^2/s$. b) Apparent diffusion coefficients $D_{app}$ obtained as in a) as a function of $\tau_b$ with fixed $\Delta = 0.04\ s$ and different maximum gradient strength $G_{max}$.

A model system ($D_a = 1 \cdot 10^{-6}\ cm^2/s$, $D_b = 1 \cdot 10^{-7}\ cm^2/s$, $p_a = 0.8$, $p_b = 0.2$, $\gamma = 267.513 \cdot 10^6\ s^{-1}T^{-1}$ and $\delta = 0.001\ s$) roughly corresponding to high temperature measurements of 3PA1BI is discussed for constant $\Delta = 0.04\ s$ and variable $\tau_b$ (see figure 17), and for constant $\tau_b = 0.01\ s$ and variable $\Delta$ (see Figure 18). Population differences directly affect the prefactors ($p'_a, p'_b$) of the exponential terms in equation 5 and the corresponding exponents through detailed balance ($\frac{p_a}{p_b} = \frac{\tau_a}{\tau_b}$). These effects are, however, comparably small for $p_a > 0.8$, i.e., for all samples of the present work.

$D_{app}$ decreases with the diffusion time $\Delta$ towards a plateau at $\Delta \geq 0.02\ s$ (see figure 18) with a plateau value depending on the choice of maximum gradients strength. For liquid samples the maximum gradient strength $G_{max}$ is often limited, as above a certain $G$ value the echo intensity is smaller than the signal-to-noise ratio. If, however, the signal-to-noise ratio limits the evaluated gradient range, higher diffusion coefficients ("complete" echo decay at low G) are less affected by the deviations than low diffusion coefficients ("complete" echo decay at high G). This and the direct dependence of $D_{app}$ on $\tau_b$ (see figure 17) result in a systematic error of the temperature dependence of $D_{app}$. For the model system the total deviation of $D_{app}$ can therefore be between 10% (for low exchange rates, low temperatures) and up to an order of magnitude (depending on the maximum gradient strength).

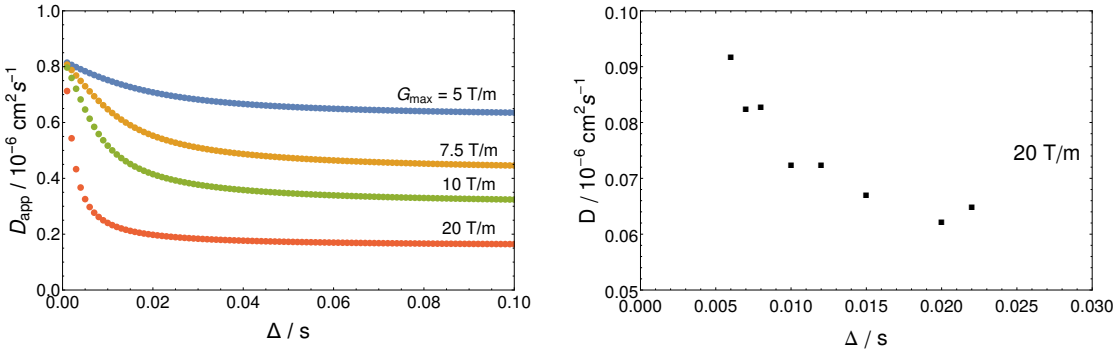


(a) Simulation (see text; $\tau_b = 0.01\ s$)

(b) 3PA1BI T= 313 K

Figure 18: Dependence of $D_{app}$ on $\Delta$ in simulation a) and experiment b).

This strong dependence of $D_{app}$ on the experimental settings, exchange rates, population differences and differences of the diffusion coefficients $D_a$ and $D_b$, results in different deviations for each investigated sample. A comparison of different samples and temperatures with the afforded accuracy of this study on structure diffusion was only possible by applying the intermediate exchange model with exchange rates obtained through lineshape analysis.

## 3.2 Influence of Exchange on the Apparent Diffusion Coefficient in PBI-PA Membranes

The numerical simulation was repeated for a model membrane with $D_b = 0\ cm^2/s$ and $D_a = 10^{-6}\ cm^2/s$, $p_a = 0.8$, $p_b = 0.2$. Stejskal-Tanner diffusion coefficients in figure 19 exhibit the same qualitative dependence on $\Delta$ and $\tau_b$ as in the case of the liquid system. The minimum plateau values do, however, not reach $D_b$ as in the liquid system; i.e., in all cases a diffusion coefficient other than zero can be fitted.

Recent literature diffusion data on PBI-PA membranes [5, 15], which include the first attempts to quantify proton diffusion in PBI-PA membranes, suffer from temperature dependent scattering and exhibit plateaus for certain temperature ranges and samples. As discussed in the main text, effects of proton exchange between polybenzimidazole and phosphoric acid, which will occur in the membranes, do not become evident in many cases through visual inspection of the echo decay in a PFG-NMR measurement. This statement is especially true for the membranes for which also the linewidth of protons associated to the polymer are wide. As argued above, the gradient and diffusion time $\Delta$ setting can result in artifacts in the temperature dependence of $D_{app}$ which are

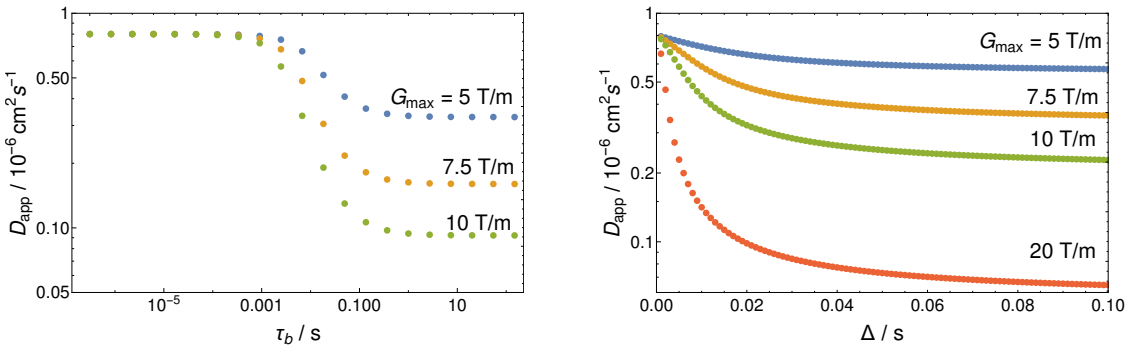


(a) $\tau_b$ dependence ($\Delta = 0.04\ s$)

(b) $\Delta$ dependence ($\tau_b = 0.01\ s$)

Figure 19: Dependence of $D_{app}$ on $\tau_b$ and $\Delta$ for a membrane ($D_b = 0\ m^2/s$).

also $\tau_b$ dependent and can exceed the differences between diffusion coefficients assumed for different membrane polymer structures and phosphoric acid contents. Experimental settings for maximum gradient strength $G_{max}$, gradient duration $\delta$, or diffusion time $\Delta$ are, however, customarily not indicated for individual measurements.

The discussed exchange model holds well for two state exchange, as it will also be found in simple phosphoric acid impregnated polybenzimidazole polymers like AB-PBI (see figure 2). Most of the PBI variations used in fuel cell membranes, however, have a more complex chemical structure than simple AB-PBI and contain benzene, pyridine or other modifications along their polymer repeat unit. Such groups may also act as proton acceptor with different basicity, thereby exchanging protons with phosphoric acid, but not directly with different proton acceptors along the polymer. Proton exchange rates are specific for each exchange partner along the polymer. A detailed description of the echo decay in PFG-NMR measurements of complex PBI-PA membranes will have to include the possibility of more than one exchange rate on the millisecond scale for exchange of protons of phosphoric acid and the polymer.

We feel future NMR studies need to address exchange of protons between phosphoric acid and the polymer, when diffusion coefficients are measured by PFG-NMR. If it is not possible to analyze the proton exchange rates between membrane and phosphoric acid, it might be required to confine diffusion studies to high concentrations of phosphoric acid and to a certain temperature range.

# References


[1] J. H. Christensen and R. B. Reed. "Design and analysis data density of aqueous solutions of phosphoric acid - measurements at 25-degrees-C". In: *Industrial and engineering chemistry* 47.6 (1955), pp. 1277–1280. DOI: 10.1021/ie50546a061.

[2] E.P. Egan and B.B. Luff. "Density of aqueous solutions of phsophoric acid - measurements at 15-degrees-C to 80-degrees-C". In: *Industrial and engineering chemistry* 47.6 (1955), pp. 1280–1281. DOI: 10.1021/ie50546a062.

[3] Anna-Liisa Huhti and Phoebus A. Gartaganis. "The composition of the strong phosphoric acids". English. In: *Candian Journal of Chemistry-Revue Canadienne de Chimie* 34.6 (1956), 785–797. DOI: 10.1139/v56-102.

[4] RF Jameson. "The composition of the strong phosphoric acids". English. In: *Journal of the Chemical Society* FEB (1959), 752–759. DOI: 10.1039/jr9590000752.

[5] J. R. P. Jayakody, S. H. Chung, L. Durantino, H. Zhang, L. Xiao, B. C. Benicewicz, and S. G. Greenbaum. "NMR studies of mass transport in high-acid-content fuel cell membranes based on phosphoric acid and polybenzimidazole". English. In: *Journal of the Electrochemical Society* 154.2 (2007), B242–B246. DOI: 10.1149/1.2405726.

[6] J. Kärger. “Zur Bestimmung der Diffusion in einem Zweibereichsystem mit Hilfe von gepulsten Feldgradienten”. In: *Annalen der Physik* 479.1–2 (1969), pp. 1–4. DOI: 10.1002/andp.19694790102.

[7] Jörg Kärger. “NMR self-diffusion studies in heterogeneous systems”. In: *Advances in Colloid and Interface Science* 23 (1985), pp. 129–148.

[8] Carsten Korte. “Phosphoric Acid, an Electrolyte for Fuel Cells – Temperature and Composition Dependence of Vapor Pressure and Proton Conductivity”. In: *Fuel Cells Science and Engineering – Materials, Processes , Systems and Technologies*. Ed. by Bernd Emonts and Detlef Stolten. Vol. 1. Wiley-VCH Verlag GmbH & Co. KGaA, 2012. Chap. 9, pp. 335–359. DOI: 10.1002/9783527650248.ch12.

[9] Klaus-Dieter Kreuer. “The role of internal pressure for the hydration and transport properties of ionomers and polyelectrolytes”. In: *Solid State Ionics* 252 (2013), pp. 93–101. DOI: 10.1016/j.ssi.2013.04.018.

[10] D.R Lide, ed. *CRC Handbook of Chemistry and Physics*. 90th. CRC Press: Boca Raton, FL, 2009.

[11] D.I. MacDonald and J.R. Boyack. “Density, electrical conductivity, and vapor pressuer of concentrated phsophoric acid”. In: *Journal of Chemical and Engineering Data* 14.3 (1969), p. 380. DOI: 10.1021/je60042a013.

[12] Ronald A. Munson. “Self-Dissociative Equilibria in Molten Phosphoric Acid”. In: *The Journal of Physical Chemistry* 68.11 (1964), pp. 3374–3377. DOI: 10.1021/j100793a045.

[13] S. Sarangapani, P. Bindra, and E. Yeager. *Physical and Chemical Properties of Phosphoric Acid*. Final Report DE-AC02-76CH00016. U.S. Department of Energy, 1978–1981.

[14] A. V. Slack, ed. *Phosphorc Acid*. Fertilizer science and technology series. M. Dekker, New York, 1968.

[15] Sophia Suarez, N. K. A. C. Kodiweera, P. Stallworth, Seonghan Yu, S. G. Greenbaum, and B. C. Benicewicz. “Multinuclear NMR Study of the Effect of Acid Concentration on Ion Transport in Phosphoric Acid Doped Poly(benzimidazole) Membranes”. In: *The Journal of Physical Chemistry B* 116.41 (2012), pp. 12545–12551. DOI: 10.1021/jp304761t.